Marine Structures 93 (2024) 103536

Contents lists available at ScienceDirect

Marine Structures

journal homepage: www.elsevier.com/locate/marstruc

Heat treatment effects on collapse of JCO-E steel pipes under external pressure: Experiments and numerical predictions

Ilias Gavriilidis [a], Aris G. Stamou [a], Christos Palagas [b], Efthimios Dourdounis [b], Nikos Voudouris [b], Athanasios Tazedakis [b], Spyros A. Karamanos [a,*]

[a] Department of Mechanical Engineering, University of Thessaly, Volos, Greece
[b] Corinth Pipeworks S.A., Thisvi, Greece

A R T I C L E I N F O

Keywords:
JCO-E pipe
Pipe manufacturing
Heat treated pipe
Offshore pipeline
Pipe collapse
Buckling propagation

A B S T R A C T

The paper examines the collapse resistance of thick-walled steel pipes, candidates for deep offshore applications, fabricated with the JCO-E process. It describes primarily a combined experimental, numerical and analytical work on the collapse of two JCO-E pipes, a 30-inch-diameter X60 pipe and a 24-inch-diameter X65 pipe, both with D/t ratio approximately equal to 20 and focuses on the effects of heat treatment. The JCO-E pipes are subjected to full-scale external pressure testing, which determines their collapse (ultimate) and propagation pressure. Prior to testing, both pipes have been subjected to a thermal heating, similar to the typical heating conditions for the application of a 3-layer coating system (i.e. 3-layer polypropylene system). Initial ovality and thickness measurements along the pipes have also been obtained. Furthermore, strip specimens, extracted from the "as fabricated" and "heat treated" pipes, have been subjected to uniaxial testing, so that the corresponding material properties are measured. In addition to experimental work, numerical calculations are performed using nonlinear finite element models that simulate the collapse testing procedure and employ the measured material properties. The experimental and numerical results on collapse and propagation pressure of the pipes are compared with the corresponding predictions of the DNV-ST-F101 standard, and the value of fabrication factor α_{fab} is discussed. Finally, a numerical study is conducted to investigate the effect of yield strength recovery, due to heat treatment, on collapse of pipes with different values of D/t.

1. Introduction

The installation of pipelines in deep water, which may exceed 2000 m, is a challenging operation associated with high hydrostatic pressure. This extreme pressure environment has the potential to cause pipe buckling and collapse in the form of cross-sectional flattening. Furthermore, in those depths propagation of the flattening pattern occurs destroying a long part of the pipeline with catastrophic consequences [1–3]. Towards safe offshore pipeline design, accurate prediction of pipe collapse resistance and post-collapse response is of major concern.

Cross-sectional buckling is initiated when the external pressure reaches a critical value (P_c), which is close to the maximum (ultimate) pressure that a pipe is capable to sustain. Upon buckling, the pipe cross-section obtains an oval shape, and the material yields at the areas of maximum hoop curvature change, resulting in a substantial reduction of pipe cross-sectional stiffness and in highly unstable post-buckling behavior. Plastic deformation concentrates at four equally-spaced locations around the circumference

* Corresponding author.
E-mail address: skara@mie.uth.gr (S.A. Karamanos).

https://doi.org/10.1016/j.marstruc.2023.103536
Received 21 June 2023; Received in revised form 22 September 2023; Accepted 27 October 2023
Available online 11 November 2023

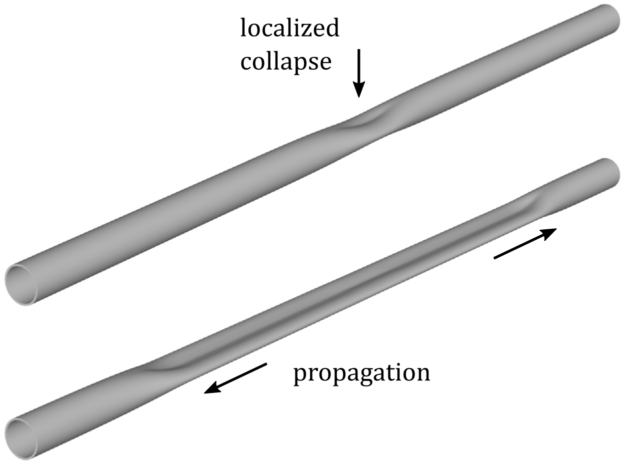

Fig. 1. Collapse of offshore pipelines and buckling propagation.

of the deformed cross-section, which act as plastic hinges [4] leading to collapse and cross-sectional flattening. The ultimate pressure that a pipe can sustain under external pressure is referred to as "collapse pressure" (P_c) and constitutes a principal parameter for offshore pipeline design [2,3]. In welded pipes, the collapse pressure is affected by several factors, related mainly to the cold forming process of the line pipe. These factors are either geometric (mainly initial cross-sectional ovality), or of material type, such as residual stresses or material anisotropy. For expanded pipes, the Bauschinger effect may also be important for determining the collapse pressure. Initially, the formation of the flattened configuration is limited to a few pipe diameters, but subsequently this configuration may propagate along the pipeline under constant pressure, flattening a very long pipeline segment, as depicted in Fig. 1. The minimum pressure required to propagate the buckle is called "propagation pressure" (P_{pr}) and it is significantly lower than the collapse pressure [2,3].

The manufacturing process of a cold-formed/expanded line pipe, such as JCO-E or UOE, introduces significant plastic strain leading to mechanical properties in the final product that are different than those of the steel plate and influence its collapse pressure. The present paper refers to the JCO-E manufacturing process, which consists of five sequential mechanical steps [5]: (a) the crimping of plate edges, (b) the J phase, where the plate is formed into a J-shape, (c) the C phase, where the deformed plate takes a quasi-round shape, (d) the O phase, where the deformed plate obtains a round shape. Subsequently the two plate ends are welded with a longitudinal seam performed with the submerged arc welding method (SAW), and finally (e) the pipe is expanded (E) with a mechanical expander [5], shown schematically in Fig. 2. Both JCO-E and UOE pipes are also referred to as "SAWL" pipes, because of the longitudinal SAW seam. Cold bending and expansion, both associated with the JCO-E manufacturing process, affect line pipe geometry, in terms of cross-sectional ovality and wall thickness, and the compressive mechanical properties in the pipe circumferential direction. These factors are crucial for the collapse strength of pipelines, and should be accounted for in the calculation of collapse pressure of pipelines installed in deep-water applications.

Previous experimental and numerical works [5–8] have shown that large-diameter line pipes, fabricated by the UOE or JCO-E process, exhibit a reduced collapse pressure capacity when compared to seamless pipes with the same D/t ratio, made of the same material. It has been recognized that the expansion phase of the manufacturing process has strong influence on collapse performance of those pipes. Expansion induces tensile plastic deformation of the pipe material in the circumferential direction of the pipe. Therefore, the compressive strength of the pipe material in the circumferential direction is significantly reduced, due to Bauschinger effect. Antoniou [9] examined this degradation of mechanical properties in expanded pipes using a rigorous finite element model. In Fig. 3, compressive stress–strain curves at two locations of a 30-inch-diameter X60 steel JCO-E pipe are plotted (inner point "A" and outer point "B" shown in Fig. 2). The stress–strain curves in Fig. 3 are obtained from coupon specimens extracted from the pipe. Fig. 3 also depicts the stress–strain response of the steel plate material used to manufacture a similar X60 pipe, and shows clearly the reduction of yield point stress because of the fabrication process.

To mitigate the reduction of compressive strength of steel material in welded pipes, a variation of the SAWL forming process has been proposed [6,8,10] in which the final expansion phase, is replaced by uniform compression to avoid reverse loading and the Bauschinger effect. However, this method is not widely used in practice. On the other hand, previous research works [7,11–17] have shown that it is possible to redeem for the compressive strength degradation of line pipe material by heat treatment. More specifically, it has been documented that a mild heat treatment process up to 250 °C temperature with a duration of a few minutes leads to partial recovery of compressive hoop strength, resulting in higher collapse capacity of the pipe. This heat treatment is imposed to the pipe during a typical epoxy coating operation for corrosion protection and thermal insulation.

The present paper focuses on the effects of heat treatment on collapse of thick-walled pipes, fabricated with the JCO-E manufacturing process. It evaluates the results from two full-scale collapse experiments on JCO-E pipes, and extends the preliminary results reported by the authors in a recent publication [18]. Prior to collapse testing, the two pipe specimens have been thermally

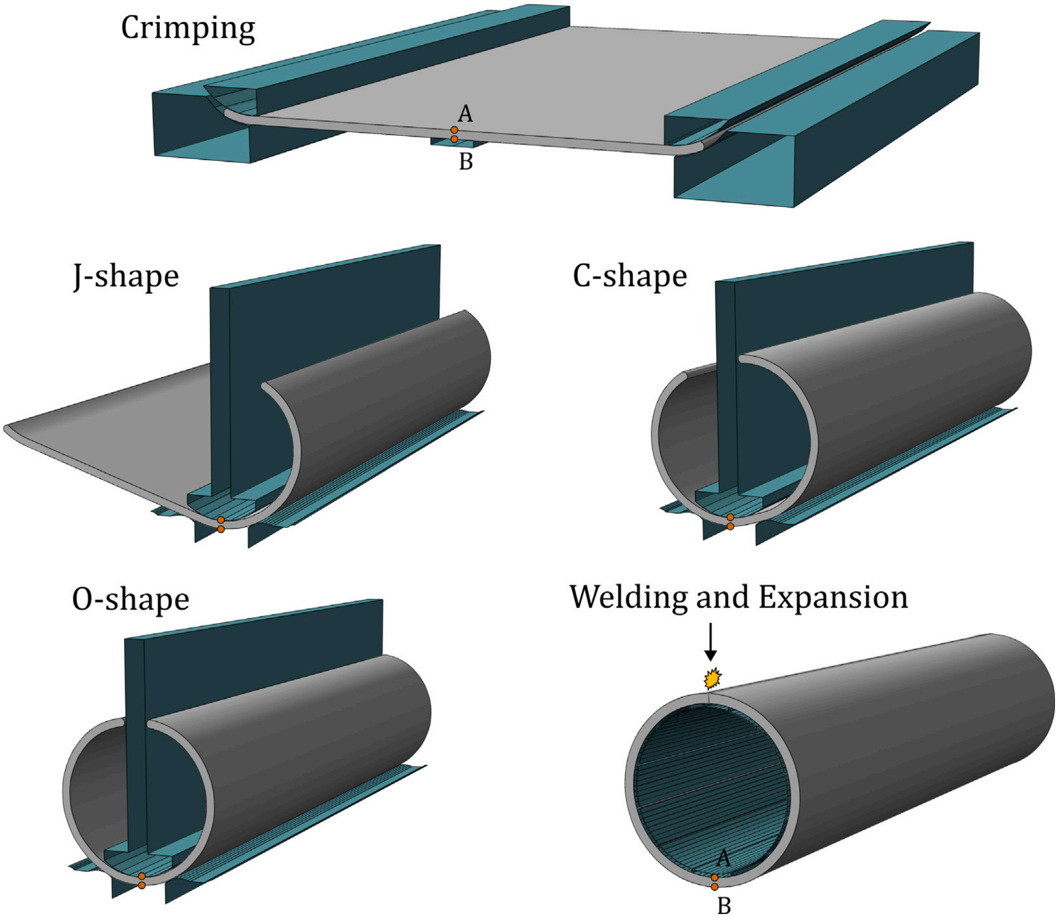

Fig. 2. Schematic representation of the JCO-E manufacturing process.

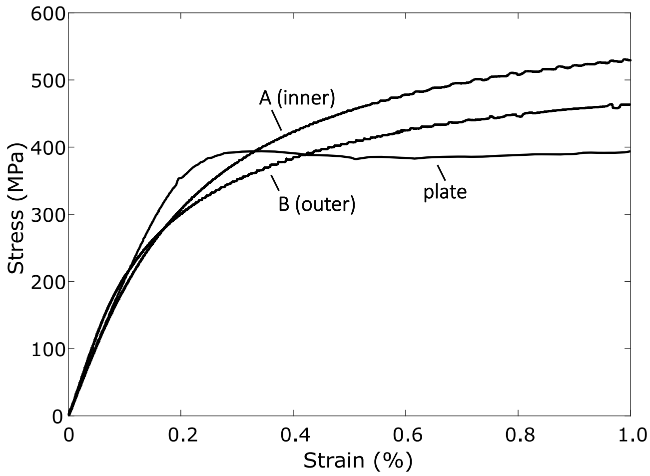

Fig. 3. Compressive stress–strain response of the X60 pipe material at the inner part (A) and the outer part (B), and stress–strain curve of the X60 plate material [9].

treated at temperature level and duration similar to the one imposed by typical coating process. Geometric measurements have been obtained along each pipe to determine their initial ovality at several cross-sections and thickness at different locations. Subsequently, collapse testing was performed, and the collapse (ultimate) pressure and the propagation pressure were measured. The full-scale tests

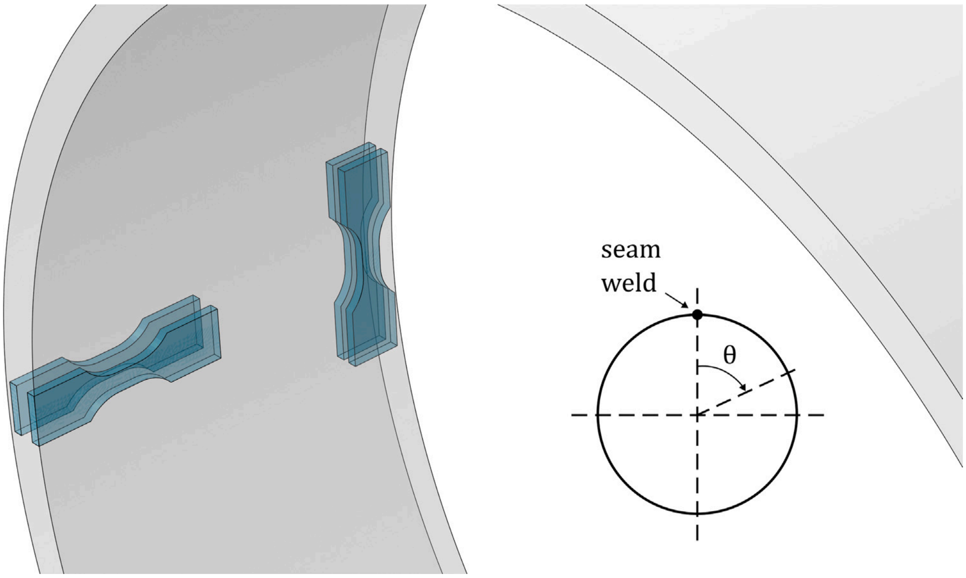

Fig. 4. Extraction of coupon specimens in the longitudinal and the transverse (circumferential) direction at the inner and outer part of the pipe specimen.

of the heat-treated steel pipes are also numerically simulated, using advanced finite element models and material data from coupon specimens extracted from the pipes under consideration. The numerical simulation results are compared with the experimental results, in terms of both collapse and propagation pressure. Numerical simulation of collapse is also performed using material data from the "as fabricated" pipes (non "heat treated") and with the results from a special-purpose simulation, presented elsewhere [9], which accounts rigorously for the effects of the manufacturing process. Furthermore, a comparison is made with the corresponding provisions of the DNV-ST-F101 [19] standard. Finally, a parametric analysis is conducted to investigate the effect of heat treatment process on the collapse pressure, considering pipes with different values of the D/t ratio.

2. Experimental procedure

The experimental program consists of both small-scale and full-scale testing on JCO-E pipes. Two full-scale collapse experiments were conducted on a 24-inch-diameter thick-walled X65 pipe and a 30-inch-diameter thick-walled X60 pipe at C-FER Technologies Inc. ("C-FER") in Edmonton, Alberta, Canada. Prior to collapse testing, each pipe specimen was subjected to thermal heating (induction), aimed at simulating the actual conditions of a typical 3-layer coating application (i.e. 3-layer polypropylene system). The axial speed of the production line was approximately 2.1 m/min and the pipe temperature ranged between 210 °C and 230 °C. A series of uniaxial tests on strip specimens, extracted from "as fabricated" (non-heat treated) and "heat treated" pipe pieces, were also conducted to obtain the properties of the "as fabricated" and the "heat treated" line pipe material.

2.1. Material properties testing

The material properties of each line pipe specimen before and after the thermal process are measured experimentally. Strip specimens were extracted from "heat treated" and "as fabricated" pieces of the JCO-E pipes, provided by the mill, using a methodology similar to the one reported by [5]. Longitudinal and circumferential coupon specimens were extracted from the outer and the inner parts of the pipe wall, as shown schematically in Fig. 4, at the 90-degree, 180-degree and 270-degree positions clockwise with respect to the weld seam.

The coupon specimens were tested in either tension or compression to obtain the corresponding material response. In total, 72 uniaxial tests were performed on specimens from the "as fabricated" and "heat treated" pipes. During the compression tests, an anti-buckling device has been employed, attached to the specimen, to prevent buckling of compressed specimens. Fig. 5 shows the stress–strain diagrams obtained from uniaxial compression tests on circumferential coupon specimens at the 90-degree inner and the outer thickness of the "as fabricated" pipe. The stress–strain curves clearly show the lower compressive strength of the outer part with respect to the compressive strength of the inner part, which is attributed to the larger tensile deformation of the outer part during manufacturing. The uniaxial tensile tests on "as fabricated" coupon specimens are shown in Fig. 6, and indicate different mechanical properties between the longitudinal and the circumferential (transverse) direction of those pipes. In particular, the stress–strain responses demonstrate a significant increase of tensile yield strength in the circumferential direction with respect to that in the longitudinal direction, attributed to strain hardening during expansion. The enhanced circumferential tensile yield strength is shown in Fig. 6(a) for the 30-inch-diameter pipe and in Fig. 6(b) for the 24-inch-diameter pipe. Furthermore, the expansion also

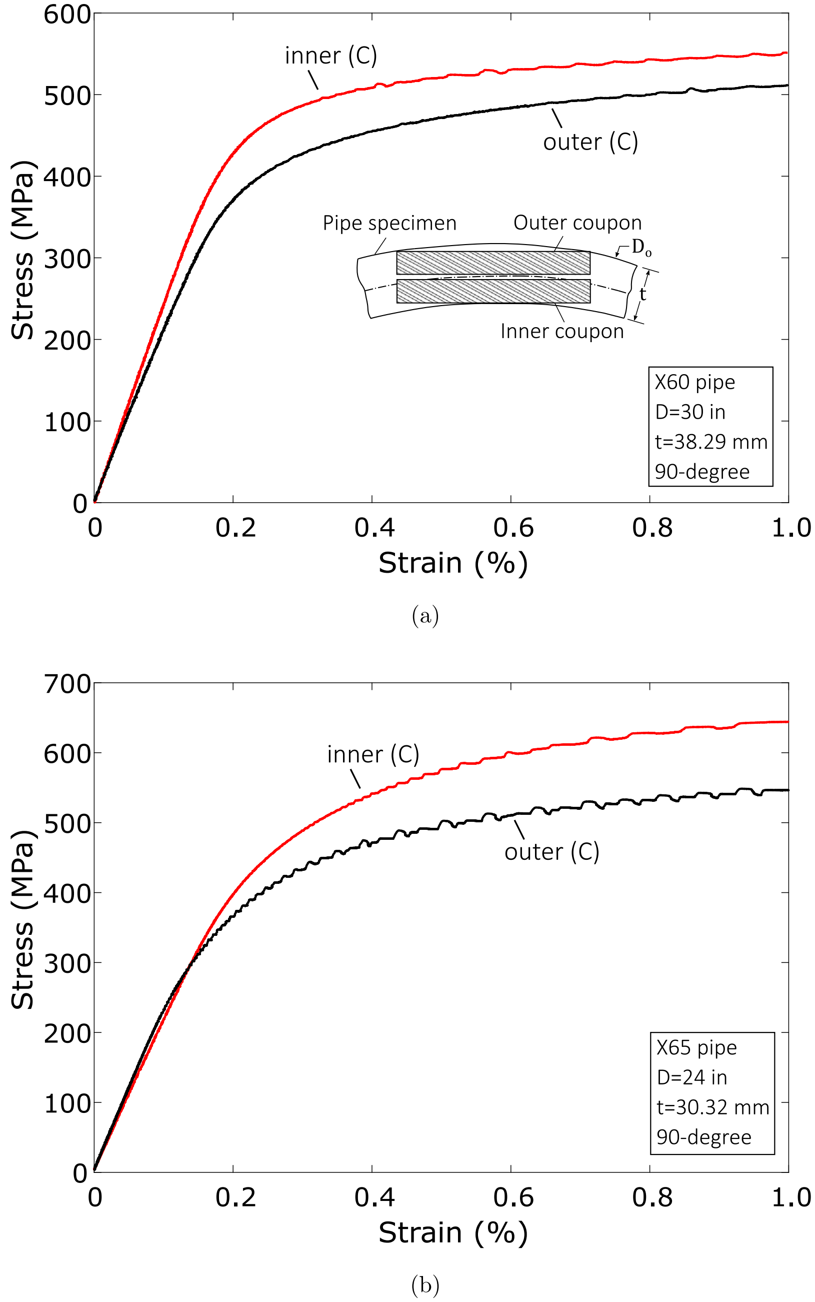

Fig. 5. Compressive (C) stress–strain curves from coupons extracted from the inner and outer part of the "as fabricated" pipe in the circumferential direction at 90-degree position: (a) 30-inch X60 pipe, (b) 24-inch X65 pipe.

affects the circumferential compressive strength. Fig. 7 presents the tensile and compressive response of both pipe materials in the transverse direction, highlighting the reduced circumferential compressive strength due to Bauschinger effect.

Fig. 8 shows the circumferential compressive stress–strain curves at the 270-degree position of the outer part of the "as fabricated" and "heat treated" pipes, and demonstrates the beneficial effects of heat treatment in terms of compressive circumferential strength recovery. The comparison of the corresponding curves indicates a compressive strength recovery in the hoop direction for both pipes because of heat treatment. The compressive yield stress (measured at 0.5% engineering strain) increases by 6.8% and 3.6% in the X60 and X65 pipes respectively, and a similar increase also occurs in the stress proportional limit. The conclusions from the present comparison are consistent with those reported by [17]. The influence of heat treatment could also be expressed in terms of the plastic work dissipated during material compression, which is increased by 6.3% and 3.8% in the X60 and the X65 material

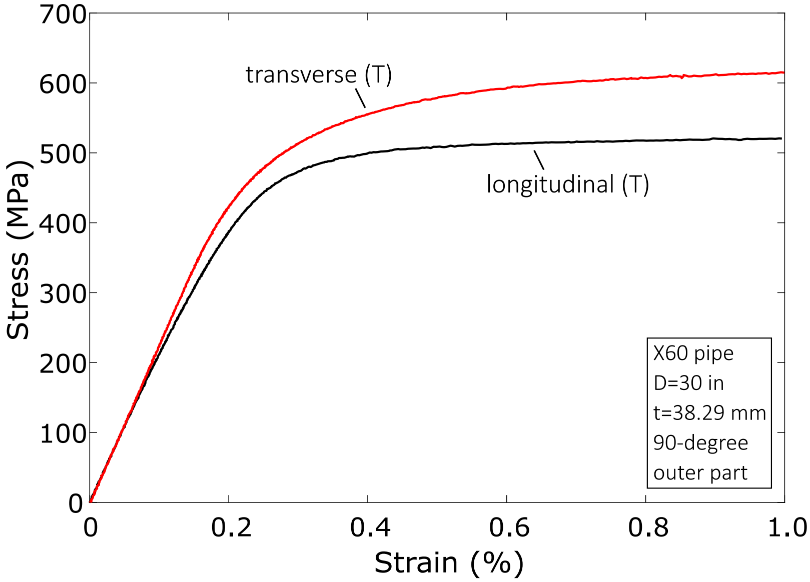

(a)

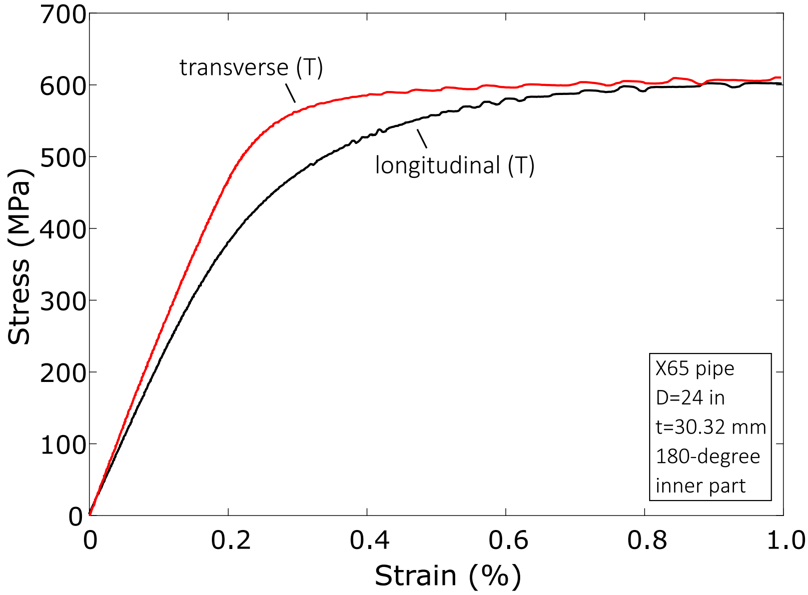

(b)

Fig. 6. Tensile (T) stress–strain curves pipe in the longitudinal and the transverse direction of the "as fabricated" pipe, extracted from: (a) the outer part at 90-degree position of the 30-inch X60 pipe, (b) the inner part at 180-degree position of the 24-inch X65 pipe.

respectively because of heat treatment. The effects of heat treatment are also evident for the inner part of the pipes, as shown in Fig. 9, where the compressive yield stress at 0.5% engineering strain increases by 8.9% and 4.1% in the X60 and X65 pipes respectively, and the corresponding plastic work is increased by 9.5% and 2.9% in the X60 and the X65 material respectively.

The compressive stress–strain curves at the outer part in the hoop direction at 90-degree, 180-degree and 270-degree for both "as fabricated" and "heat treated" pipes are averaged, and the resultant stress–strain curves are considered in the finite element model, described in Section 3. Table 1 summarizes the yield stress values of the averaged stress–strain curves before and after the heat treatment. In this table, σ_y is the stress at 0.5% engineering strain (denoted as "yield stress"). There is 5.6% and 4.6% increase of the yield stress in X60 and X65 grade material, respectively, because of heat treatment. The beneficial effect of heat treatment

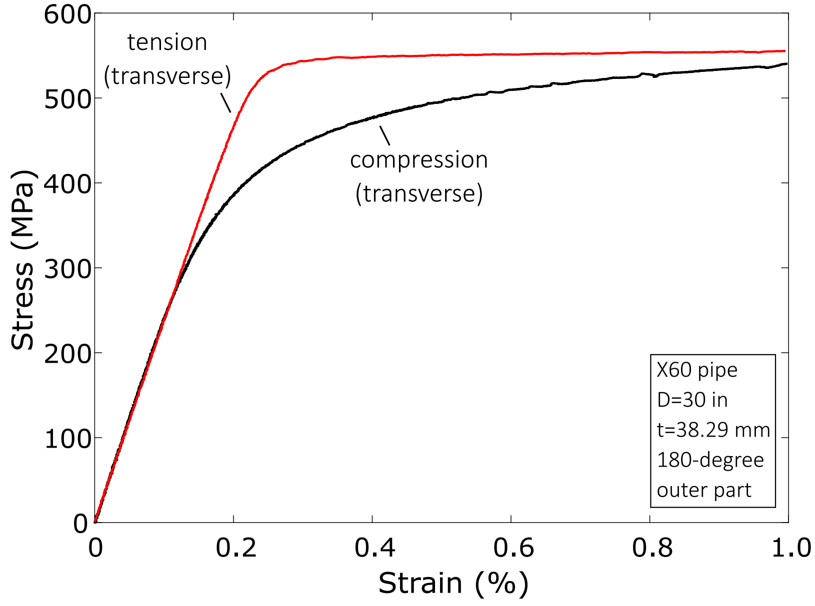

(a)

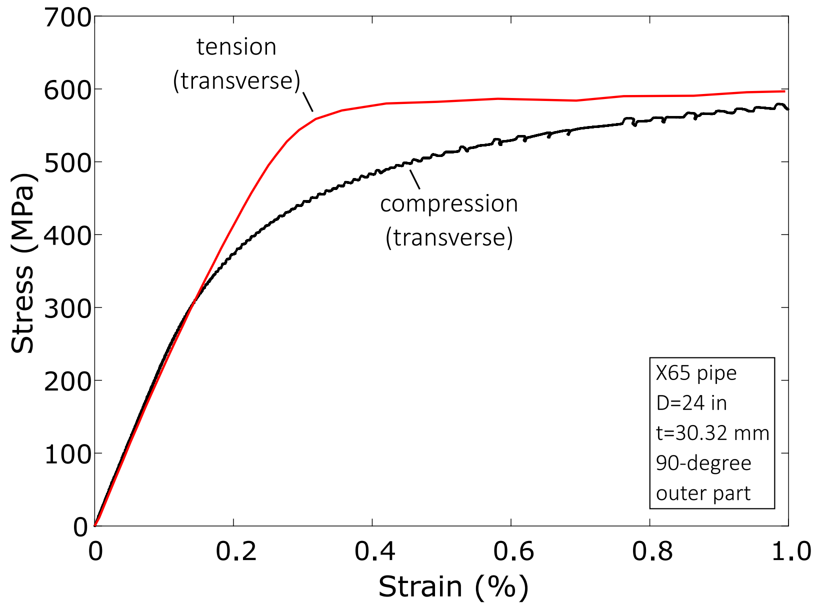

(b)

Fig. 7. Tensile and compressive stress–strain responses in the circumferential direction (coupons extracted from outer part of the "as fabricated" pipe): (a) at 180-degree position of the 30-inch-diameter X60 pipe and (b) at 90-degree position of the 24-inch-diameter X65 pipe.

can be also quantified by the amount of plastic work dissipated during uniaxial compression, which is increased by 6.3% and 3.9% for the X60 and the X65 pipe material, respectively.

2.2. Full-scale collapse testing

The collapse experiments of the two pipe specimens were conducted in the Deepwater Experimental Chamber (DEC) of C-FER Technologies. The DEC has pressure capacity 55.2 MPa (8000 psi or 551.6 bar), inside diameter of 1.2 m, total inside length of 10.3 m, and has been extensively used for numerous collapse tests in the last three decades [12,14]

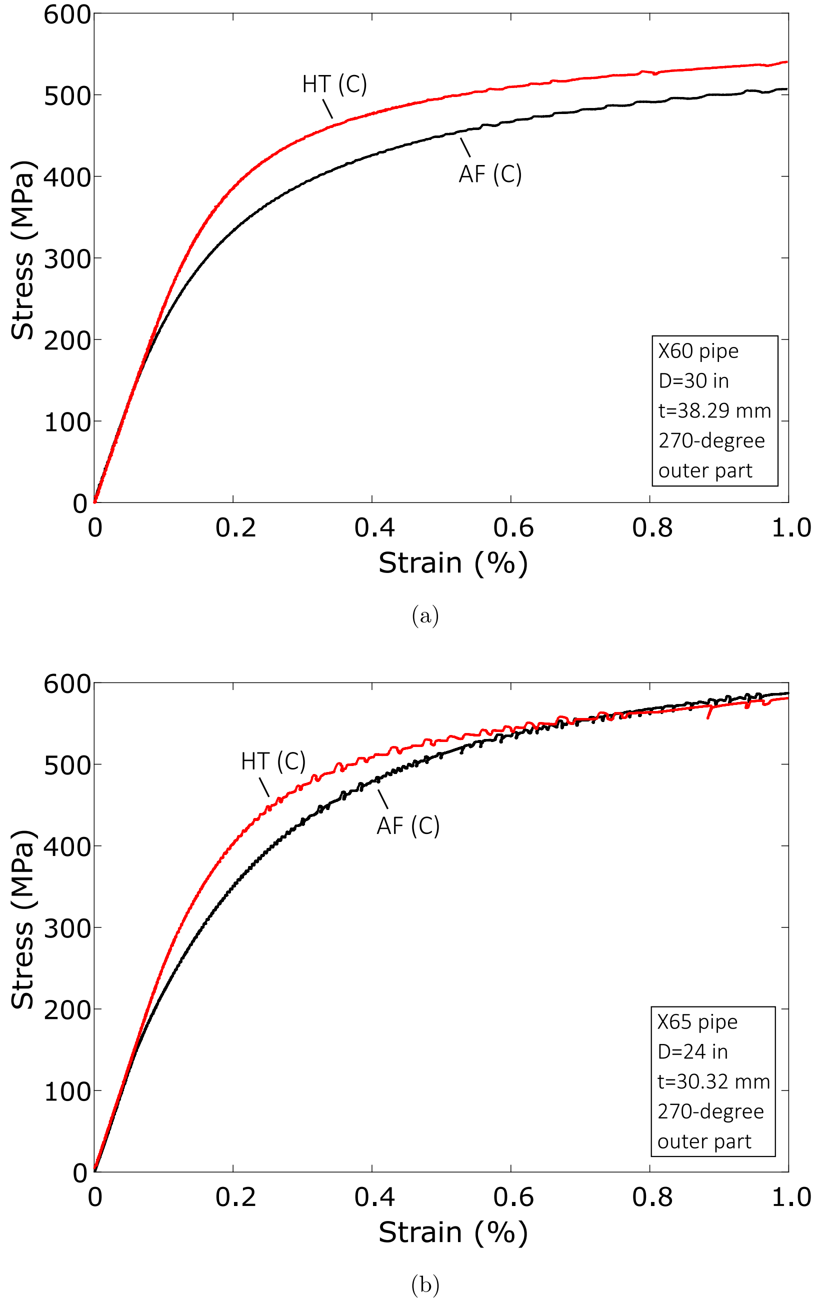

Fig. 8. Compressive (C) stress–strain responses at 270-degree position (coupons extracted from outer part of the pipe) in the circumferential direction before (AF) and after heat treatment (HT); (a) 30-inch-diameter X60 pipe and (b) 24-inch-diameter X65 pipe.

The pipe specimens were ten diameters long. Ovalization and thickness measurements of the pipes were obtained before testing using state-of-the-art software, and signal equipment. Each specimen was marked at 16 locations circumferentially and 9 stations longitudinally, and a grid of 144 (16 × 9) points was created, as shown in Fig. 10, allowing for measuring the external diameter (D_o) and the wall thickness (t) at numerous locations prior to testing. The outer diameter was measured with a micrometer, and the initial ovality (O_o) of the pipe at a specific cross-section was calculated from these measurements, using the following expression from DNV-ST-F101 [19]:

$$O_o = \frac{D_{o,max} - D_{o,min}}{D_o} \tag{1}$$

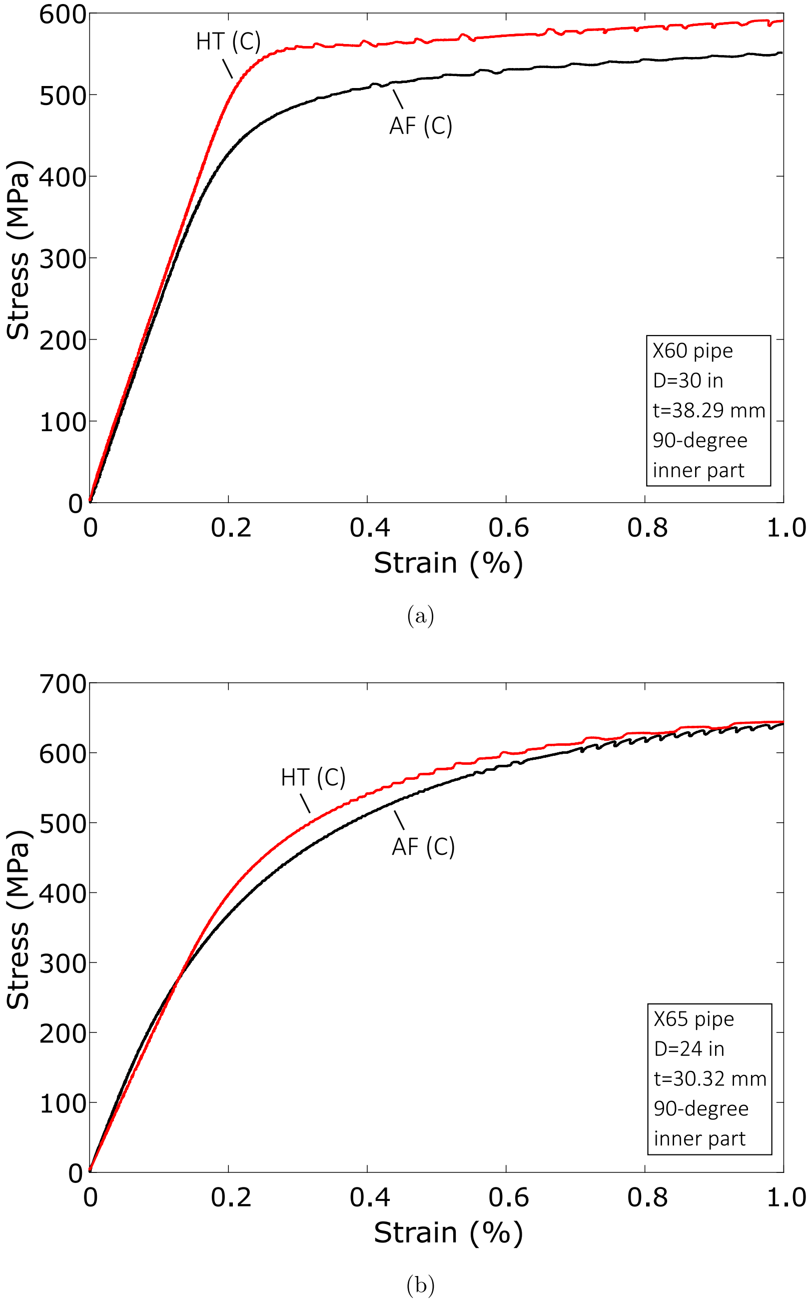

Fig. 9. Compressive (C) stress–strain responses at 90-degree position (inner part of the pipe) in the circumferential direction before (AF) and after heat treatment (HT); (a) 30-inch X60 pipe and (b) 24-inch X65 pipe.

where D_o is the nominal outer diameter, $D_{o,max}$ is the maximum measured outer diameter, and $D_{o,min}$ is the minimum measured outer diameter at the same cross-section. The geometric characteristics of each pipe were measured, such as the total pipe length, the wall thickness, the outer diameter of the pipes and the cross-sectional ovality, using a calibrated ultrasonic probe. The geometric measurements are summarized in Table 2.

Each end of the pipe was capped, and attached to a rolling device inside the chamber. Subsequently, the chamber was filled with water, and using a water pump, water was introduced into the chamber, with “capped” or “hydrostatic” conditions at the pipe ends. Upon collapse, water input inside the chamber was further continued, so that the collapse pattern propagates along the specimen length, and the propagation pressure is measured. The change of volume enclosed by the pipe during the test was measured by monitoring the amount of water pumped into the chamber, at each step. The test values of collapse and propagation pressure

Table 1
Material properties of X60 and X65 steel pipe specimens at the outer part of both pipes before (“as fabricated” AF) and after heat treatment (“heat treated” HT). These properties obtained by averaging the outer experimental compressive stress–strain curves.

Pipe specimen	Yield stress σ_y (MPa)		
	AF[a]	HT[a]	Nominal
24-inch (grade X65)	503	526	448
30-inch (grade X60)	464	490	414

[a] At 0.5% total strain.

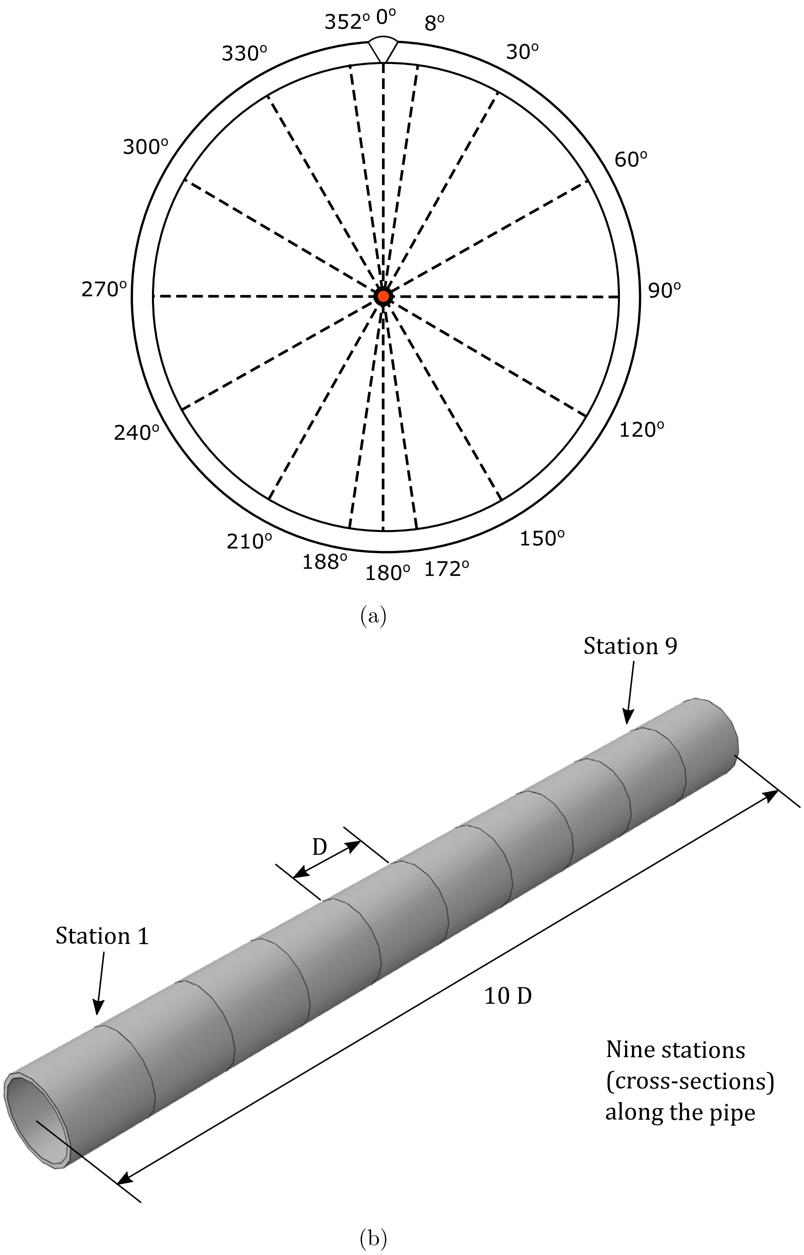

Fig. 10. Grid of points on the pipe surface for measuring diameter, ovality and thickness (a) in the circumferential direction and (b) in the longitudinal direction.

Table 2
Measurements of wall thickness, cross-sectional ovality, pipe diameter of the 30-inch and the 24-inch diameter pipe prior to collapse test.

Measurements	Specimen 24-inch OD	Specimen 30-inch OD
Wall Thickness (mm)		
Maximum Wall Thickness	30.51	38.61
Minimum Wall Thickness	30.15	37.90
Average Wall Thickness	30.32	38.29
Diameter (mm)		
Maximum Diameter	610.7	762.0
Minimum Diameter	608.5	760.6
Average Diameter	609.5	761.4
Ovality (%)		
Maximum Ovality	0.300	0.140
Minimum Ovality	0.244	0.060
Average Ovality	0.272	0.089
Length and Circumference (mm)		
Average Length	6204	7635
Average Circumference	1918	2395

Table 3
Collapse pressure (in MPa) of the 24-inch and 30-inch diameter pipe specimens considering capped and fixed ends; experimental values, numerical results and DNV-ST-F101 predictions.

Pipe specimen	Boundary condition	Numerical simulation			Experimental value	DNV $\alpha_{fab} = 0.85$	DNV (HT) $\alpha_{fab} = 1$
		AF	HT	2D			
24-inch OD	Capped	36.3	41.8	–	40.3	36.8	42.5
	Fixed	36.0	41.1	–	–		
30-inch OD	Capped	39.2	44.3	38.4	45.4	35.0	41.4
	Fixed	38.5	43.4	37.5	–		

Table 4
Propagation pressure (in MPa) of the 24-inch and 30-inch diameter pipe specimens considering capped and fixed ends; experimental values, numerical results ($L = 14D_o$) and DNV-ST-F101 predictions.

Pipe specimen	Boundary condition	Numerical simulation HT	Experimental value	DNV (HT) $\alpha_{fab} = 1$
24-inch OD	Capped	9.4	9.3	10.2
	Fixed	9.4		
30-inch OD	Capped	9.2	9.1	9.7
	Fixed	9.3		

are depicted in Tables 3 and 4, while the post-test configuration of the collapsed and flattened 30-inch-diameter pipe specimen is presented in Fig. 11. Fig. 11 also depicts the collapse configurations of the numerical simulations, described in Section 3, for comparison. A similar collapse configuration was also obtained for the 24-inch pipe specimen.

3. Description of finite element model

Numerical simulations of collapse and buckle propagation are conducted using general-purpose finite element package ABAQUS/ Standard [20]. The analysis has a dual purpose: first, to simulate the experimental procedure and second, to elucidate some aspects of pipe behavior in connection with material properties. The finite element model accounts for both geometric and material non-linearities. The pipe material is described through elastic–plastic J_2 (von Mises) flow plasticity model. Fig. 12 depicts the finite element model of the 30-inch-diameter line pipe, which simulates the collapse process of the line pipe during the full-scale tests in the pressure-chamber. The model is five outer diameters long ($L = 5D_o$), simulating half of the pipe specimen length and considers a quarter of the cross section of the line pipe due to double symmetry. Symmetry conditions with respect to the $x - z$ and $y - z$ planes are used, as shown in Fig. 12. The x–y plane symmetry at the $z = 0$ plane, accounts for the ten-diameter-long specimen tested in full-scale, as described in Section 2.2, allowing only in-plane motion on the corresponding nodes. The end section at $z = L$ plane is "capped" preventing cross-sectional ovalization but allowing for axial movement, representing the boundary conditions imposed during the test. In that section, a compressive axial force F_p is applied considering the effect of hydrostatic pressure on the caps, which is equal to the product of the external pressure P times the area of the capped-end plate A of the specimen ($F_p = PA$). Additional analysis is also performed applying fixed ends, which is a more realistic loading pattern for an offshore pipeline.

The thick-walled pipes are modelled with 20-node reduced-integration solid elements, denoted in ABAQUS as C3D20R. Twenty-five elements are used around the quarter pipe cross-section, with one hundred elements in the longitudinal direction of the pipe

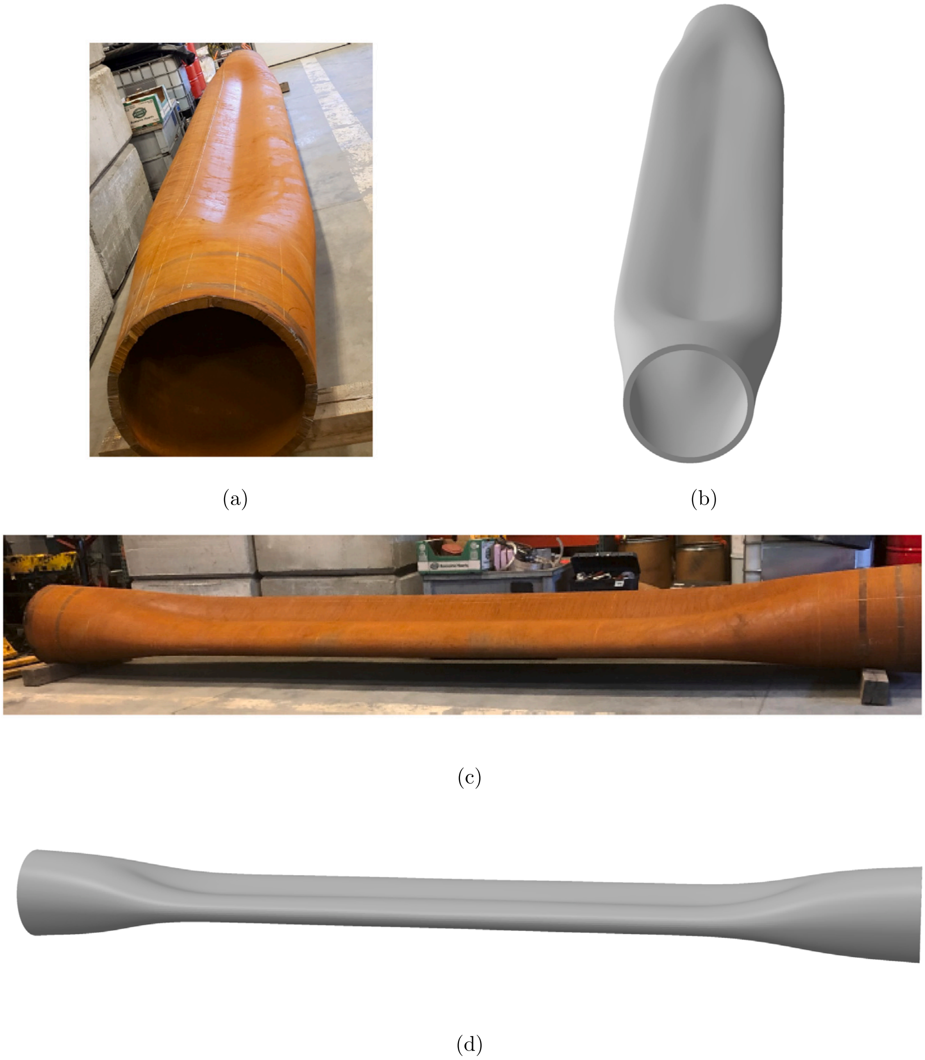

Fig. 11. Deformed (collapsed) configuration of the 30-inch-diameter pipe: (a), (c) full-scale collapse test; (b), (d) numerical simulation.

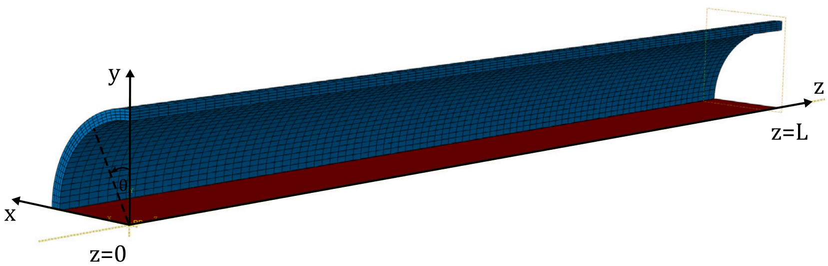

Fig. 12. Three-dimensional numerical model of the 30-inch diameter line pipe specimen.

and four elements through the pipe wall thickness. The initial geometry of the numerical models in terms of diameter, ovality and thickness are based on the average measurements presented in Table 2. The cross-section at the $z = L$ end has an oval shape, with amplitude equal to the minimum ovality measured in the corresponding pipe specimen, shown in Table 2, whereas the cross-section at $z = 0$ has the maximum ovality depicted in Table 2. In the 30-inch-diameter pipe model, the ovality O_o in the symmetry section ($z = 0$) is equal to 0.14%, and reduces linearly to 0.06% at the end section ($z = L$). In the 24-inch-diameter pipe model, the ovality in the symmetry section is equal to 0.30%, and gradually reduces to 0.24% at the end section.

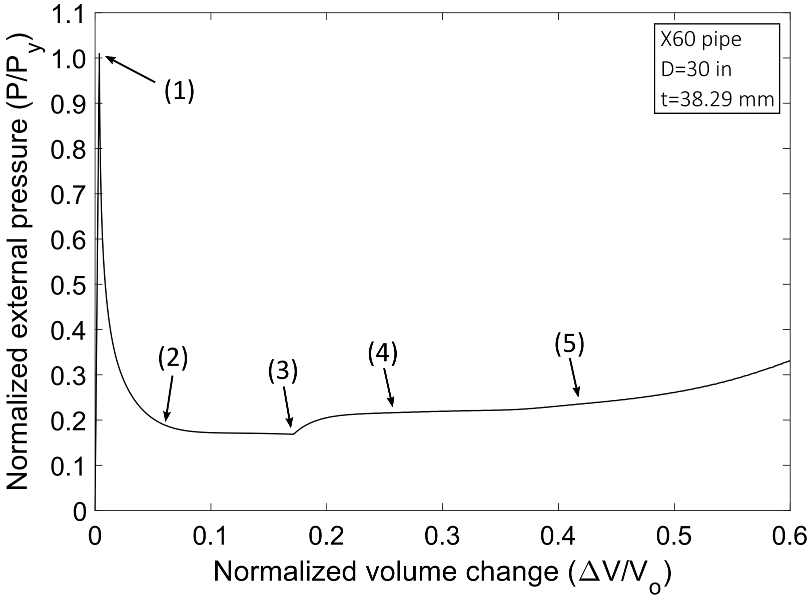

Fig. 13. External pressure vs. volume change diagram of the "heat treated" 30-inch-diameter pipe; finite element simulation.

The model includes an analytical rigid surface at $x - z$ plane ($y = 0$), depicted in Fig. 12, to account for contact of the top and the bottom side of the pipe inner surface during post-collapse flattening and buckle propagation. A frictionless surface-to-surface interaction is assumed, assigning the horizontal plane as "master" surface and the inner surface of the pipe as "slave" surface. Moreover, the "direct" method for hard pressure-overclosure is applied, also employed by the authors in a previous publication [18].

The circumferential compressive strength of the material governs pipe collapse strength under external pressure. Therefore, the averaged compressive stress–strain curve at the outer part, where the lowest compressive material strength occurs due to the longer tensile deformation during fabrication, is considered in the numerical simulation of both pipes. The yield stress values of the averaged stress–strain curves of the "as fabricated" and "heat treated" pipes are presented in Table 1. In all analyses, the values of Young's modulus (E) and Poisson's ratio (ν) are considered equal to 207 GPa and 0.3, respectively.

4. Numerical predictions of collapse and propagation pressure

The full-scale collapse experiments of the two heat-treated specimens are simulated using the finite element (FE) model, described in the previous section and the numerical predictions of collapse pressure are compared with the experimental values. Additional numerical results are obtained for both pipes using the material properties before and after heat treatment, to investigate the effects of compressive strength recovery on the collapse pressure ("as fabricated" pipes).

4.1. Collapse pressure

Fig. 13 presents the pressure–volume diagram for the 30-inch diameter pipe, which shows the variation of applied external pressure (P) with respect to the volume change enclosed by the pipe (ΔV). The value of P is normalized by the yield pressure of the pipe (P_y):

$$P_y = 2\sigma_{y,n} \frac{t}{D_o - t} \tag{2}$$

where $\sigma_{y,n}$, D_o and t are the specified minimum yield stress (SMYS) of X60 steel material (60 ksi or 415 MPa), the nominal outer diameter value of the 30-inch-diameter pipe, and the wall thickness respectively. The average value of pipe wall thickness from real measurements obtained before the test (Section 2.2) is considered in each pipe (Table 2). Furthermore, the averaged compressive stress–strain curves at the outer part of the pipe after heat treatment are employed, and capped-end boundary conditions are applied, considering the effect of hydrostatic pressure. The value of ΔV is normalized by the initial volume enclosed by the pipe (V_o). The volume enclosed by the pipe in each increment during the analysis is calculated in a post-processing phase, using the node coordinates on the inner surface of the pipe.

The numbers in brackets on the pressure–volume diagram of Fig. 13 correspond to the deformed configurations of the 30-inch-diameter pipe shown in Fig. 14. The pressure increases until the maximum (collapse) pressure is reached [stage "(1)"]. Upon collapse, the pipe becomes highly unstable and post-buckling deformation is governed by a "four-plastic hinge" collapse mechanism, resulting in a significant reduction of pressure, represented by stage "(2)" in the post-buckling path. Eventually, a minimum value of pressure

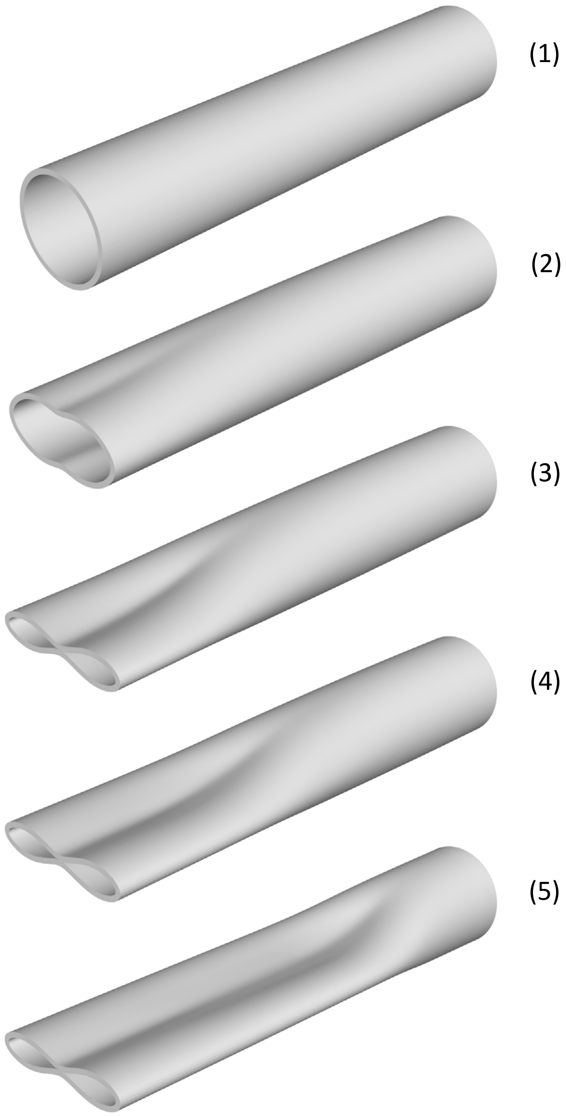

Fig. 14. Deformation sequence of the 30-inch-diameter X60 pipe from the stage of maximum pressure to buckling propagation (finite element simulation); the configuration numbers refer to the corresponding points on the pressure–volume diagram in Fig. 13.

is reached at stage "(3)", corresponding to first contact of two opposite sides of the collapsed cross-section. Subsequently, a small increase in pressure occurs from stage "(3)" to stage "(4)" and the buckle starts propagating along the pipe under nearly constant pressure, as depicted in the deformed configuration of stage "(5)". Following that stage, the pressure begins to rise, due to the influence of capped end conditions at $z = L$. The response of the 24-inch pipe follows a pressure–volume diagram analogous to the one in Fig. 13, with post-buckling configurations similar to the ones presented in Fig. 14.

The numerical and the experimental results in terms of collapse pressure are in very good agreement for both pipe specimens. The numerical values of collapse pressure are 41.8 MPa and 44.3 MPa for the 24-inch-diameter and the 30-inch-diameter pipe respectively, and compare quite well with the corresponding experimental results, namely 40.3 MPa and 45.4 MPa for the 24-inch and 30-inch pipe, respectively. The difference between the numerical predictions and the experimental values is less than 4%. The above good comparison indicates that accurate predictions of the collapse pressure can be obtained, using an appropriate compressive stress–strain material curve in the finite element calculations, and initial pipe geometry based on real measurements.

The pressure–volume diagram obtained numerically for the 30-inch-diameter pipe (Fig. 13) is compared with the corresponding experimental pressure–volume response recorded during the full-scale collapse test, as shown in Fig. 15. The comparison is very satisfactory, not only in terms of collapse pressure, but also in the post-buckling regime. The abrupt descending branch of the experimental curve is due to sudden depressurization of the chamber immediately after reaching the maximum pressure, which required additional pumping of water to restore the external pressure level. The abrupt drop of pressure during the experiment

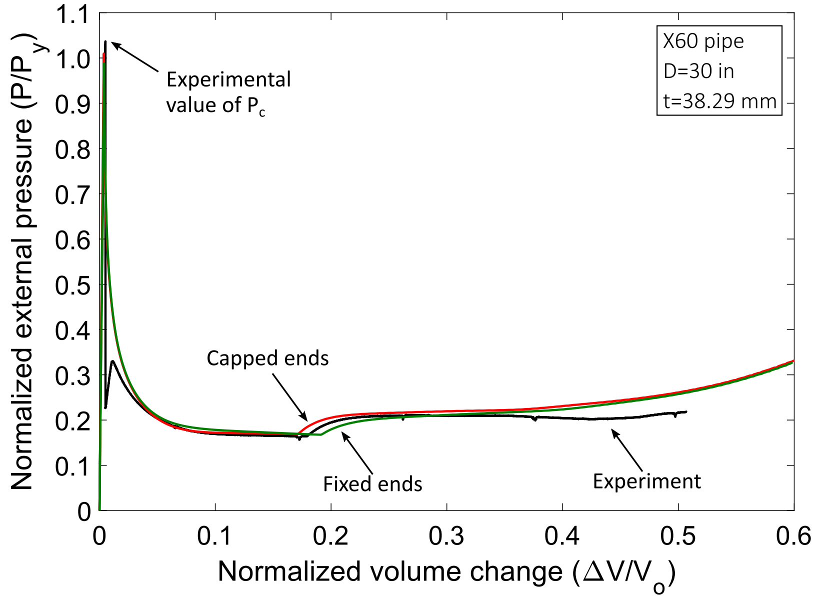

Fig. 15. External pressure variation with respect to the volume change for the "heat treated" 30-inch-diameter pipe; comparison between numerical simulations and full-scale experiment.

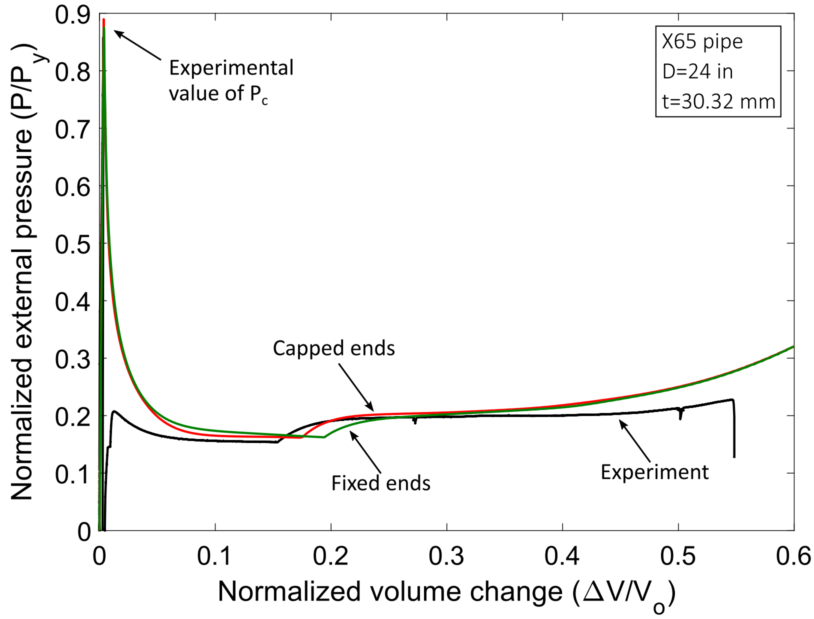

Fig. 16. External pressure variation with respect to the volume change for the "heat treated" 24-inch-diameter pipe; comparison between numerical simulations and full-scale experiment.

has also been reported in previous works [21]. Fig. 15 also presents the pressure–volume diagram in the case of fixed boundary conditions at the end of the pipe model, which represent a more realistic scenario during collapse of a long pipeline at the seabed and will be used later in the paper for parametric study. In this case, the collapse pressure is 43.4 MPa, which is somewhat lower than the corresponding value obtained for hydrostatic conditions.

Furthermore, Fig. 16 presents the pressure–volume curve in the case of fixed boundary conditions at the end of the 24-inch-diameter pipe model compared to the capped ends boundary conditions and the experimental curve. In this case, the collapse pressure is 41.1 MPa, which is somewhat lower than the collapse pressure value for hydrostatic conditions. The numerical results show that the collapse pressure prediction of both pipes in case of capped ends is higher than in case of fixed ends. This is attributed to the von Mises yield criterion, where the material yields at higher hoop stress in case of bi-axial compression. Fig. 16 shows a

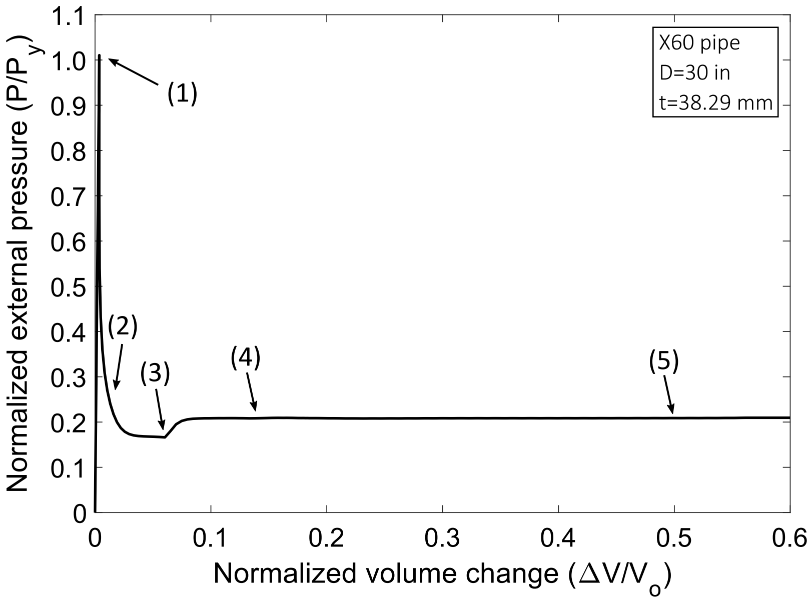

Fig. 17. External pressure variation vs. volume change diagram for the "heat treated" 30-inch-diameter pipe (numerical simulation, $L = 14D$); the marked points depicted correspond to (1) ultimate pressure, (2) post-buckling, (3) contact, (4) and (5) steady-state propagation.

zero drop during the experiment, which is attributed to an end cap failure immediately after the pipe collapsed. The test stopped and the buckling propagation process was completed once the end cap was replaced.

4.2. Propagation pressure

Fig. 15 shows a fairly good agreement between the numerical simulations and the value of propagation pressure measured experimentally. The numerical prediction of the propagation pressure for the 30-inch diameter pipe ($L = 5D_o$), is 9.6 MPa, when capped boundary conditions are used in the model, and 9.3 MPa with fixed boundary conditions. The numerical predictions compare well with the experimental measurement of propagation pressure for 30-inch diameter pipe (9.1 MPa). Fig. 16 presents the pressure–volume diagram in the case of fixed boundary conditions at the end of the 24-inch-diameter pipe model ($L = 5D_o$) compared to the capped-end boundary conditions and the experimental curve. In this case, the propagation pressure is 9.7 MPa and 9.6 MPa for capped ends and fixed ends, respectively, and compare very well with the corresponding experimental value (9.3 MPa). However, a steady state deformation of both pipes during buckle propagation is difficult to obtain in this analysis because of the short length of this model. The results show that considering a five-diameter long model, the buckle reaches the pipe ends before a constant value of buckle propagation is reached, resulting in increase of the applied pressure. Therefore, an additional numerical model is developed with pipe length equal to fourteen outer diameters ($L = 14D_o$), which simulates steady state buckle propagation in a long pipe in a more efficient manner. Apart from its length, the model is similar to the one depicted in Fig. 12 (described in detail in Section 3) in terms of geometric and material properties and finite element mesh density. Capped boundary conditions are applied on the $z = L$ plane of the model. The use of this 14-diameter long model allows for the buckle to propagate under steady-state conditions over a significant length of pipe without influence of boundary conditions and, therefore a more reliable numerical prediction of the propagation pressure is obtained. Fig. 17 depicts the equilibrium diagram of applied external pressure versus the corresponding volume change for the 30-inch-diameter pipe. The numbers on the pressure–volume diagram of Fig. 17 correspond to the deformed configurations of the collapsed pipe in Fig. 18. The diagram has many similarities with the diagram in Fig. 13, obtained with the five-diameter model-long. However, after the increase of external pressure from the touchdown point of stage "(3)" to stage "(4)", the steady state reached by the flattened pipe is more extended and the buckle travels a longer distance under constant external pressure before reaching the pipe end. Using a similar numerical model ($L = 14D_o$), the pressure–volume diagram has been obtained for the 24-inch pipe. The diagram is similar to the one shown in Fig. 17, but is not shown in the paper for the sake of brevity.

Using the long model ($L = 14D_o$) and assuming capped boundary conditions, the propagation pressure is predicted equal to 9.4 MPa and 9.2 MPa for the 24-inch and 30-inch pipe, respectively. These values are in very good agreement with the experimental values reported from the full-scale tests (9.3 MPa for the 24-inch pipe and 9.1 MPa for the 30-inch pipe). Additional analyses are performed with this long model considering fixed boundary conditions, resulting in 9.4 MPa and 9.3 MPa for the 24-inch and 30-inch pipe, respectively, and this indicates that the end conditions, ("capped" or "fixed") have a negligible effect on the value of propagation pressure.

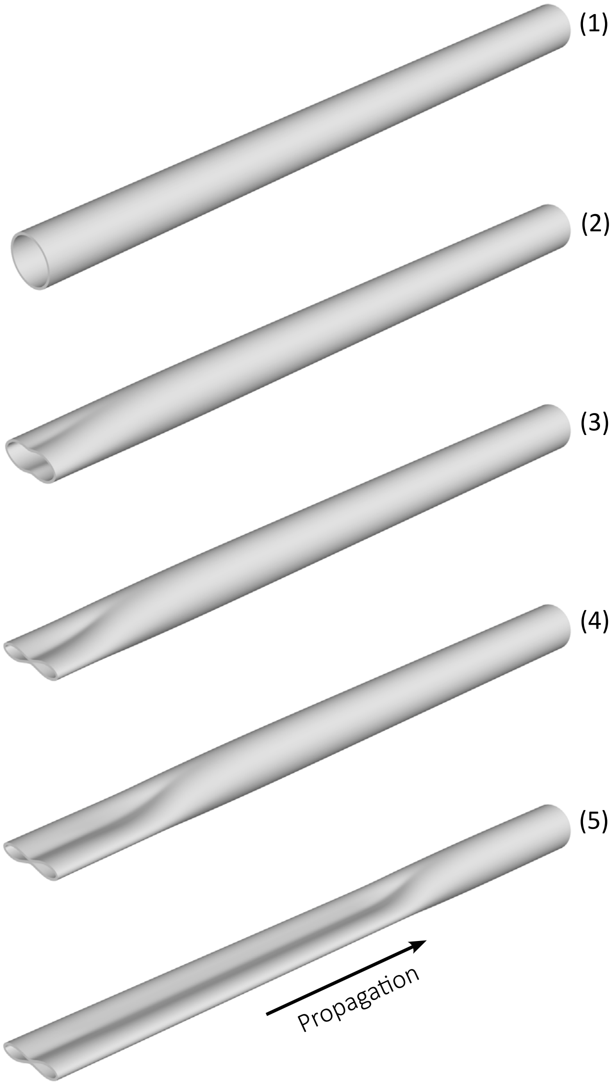

Fig. 18. Deformation sequence of the 30-inch-diameter X60 pipe from maximum pressure to buckling propagation; the configuration numbers refer to the corresponding points on the pressure–volume diagram in Fig. 17 (numerical simulation, $L = 14D_o$).

4.3. Evaluation of heat treatment effects on the collapse pressure and propagation pressure

The finite element models of the previous sections ($L/D_o = 5$ and $L/D_o = 14$) are employed to highlight the influence of heat treatment on pipe collapse resistance. Towards this purpose, the corresponding stress–strain curves before and after heat treatment are considered. Analyses have been performed with both "capped" and "fixed" end conditions for the sake of completeness. Fig. 19 shows the variation of applied external pressure in terms of volume change for the "as fabricated" and the "heat treated" pipes, and indicates the beneficial effect of mild heat treatment process on collapse. The collapse pressure of the heat treated 30-inch pipe is increased by approximately 13% for both end conditions, compared to the "as fabricated" specimen, while the corresponding increase for the 24-inch pipe is 15%. The results show that in both pipes the collapse pressure increase due to the beneficial effect of mild heat treatment is independent of end conditions. Furthermore, capped ends increase the stiffness as shown by the slope of the diagram. Table 3 summarizes the experimental results and the numerical predictions of collapse pressure considering capped and fixed end conditions.

For comparison purposes, the numerical prediction of collapse pressure is also obtained from a two-dimensional (2D) finite element model, which accounts rigorously for the JCO-E manufacturing process in the first part of the analysis [9] and is also included in Table 3. The collapse pressure from this model is 38.4 MPa and 37.5 MPa for capped and fixed ends, respectively, and refers to the "as fabricated" pipe. In that rigorous model, hereafter "2D manufacturing/collapse" model, an expansion strain equal to 1.30% is considered, which is an approximate value of the expansion strain applied during the production of the pipe in the mill.

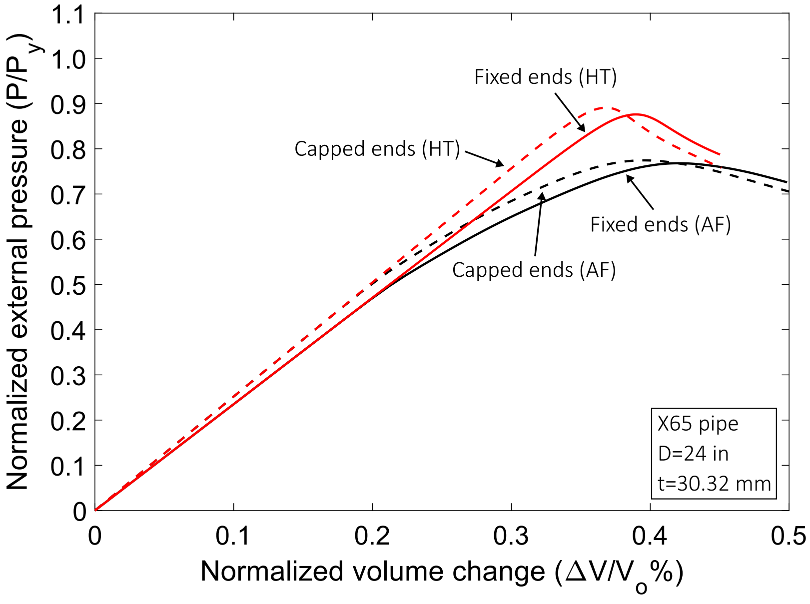

(a)

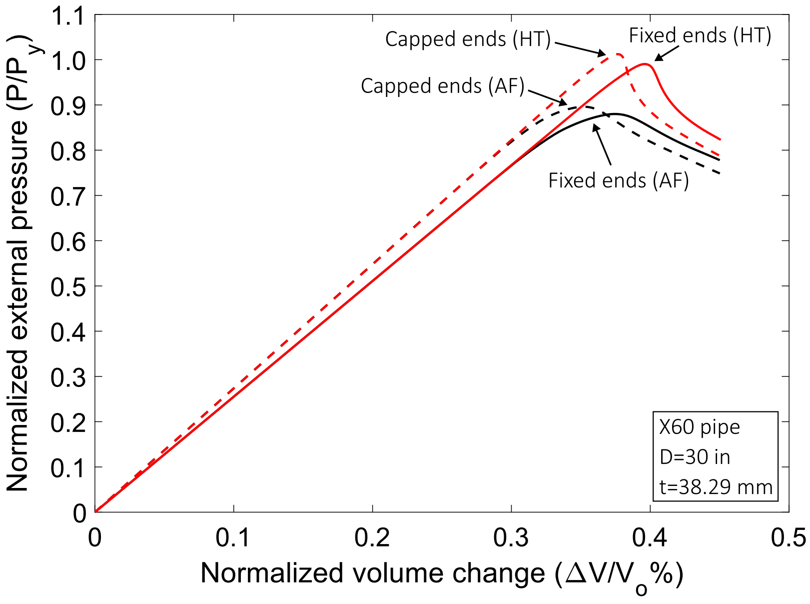

(b)

Fig. 19. Diagram of external pressure vs. volume change enclosed by the deforming pipe; (a) 24-inch-diameter and (b) 30-inch-diameter pipe.

Furthermore, in that model, during the collapse stage of the analysis, an axial compressive force is applied, which represents the effect of capped end conditions during external pressurization. The comparison of collapse pressure predictions from the 3D ("as fabricated") model and the 2D manufacturing/collapse model is very satisfactory.

In Table 3 the numerical and experimental values of collapse pressure are also compared with the collapse pressure prediction (P_c) of the DNV-ST-F101 [19] standard, calculated from the solution of the following third-degree algebraic equation:

$$\left(P_c - P_{el}\right)\left(P_c^2 - P_p^2\right) = P_c P_{el} P_p O_o \frac{D_o}{t} \tag{3}$$

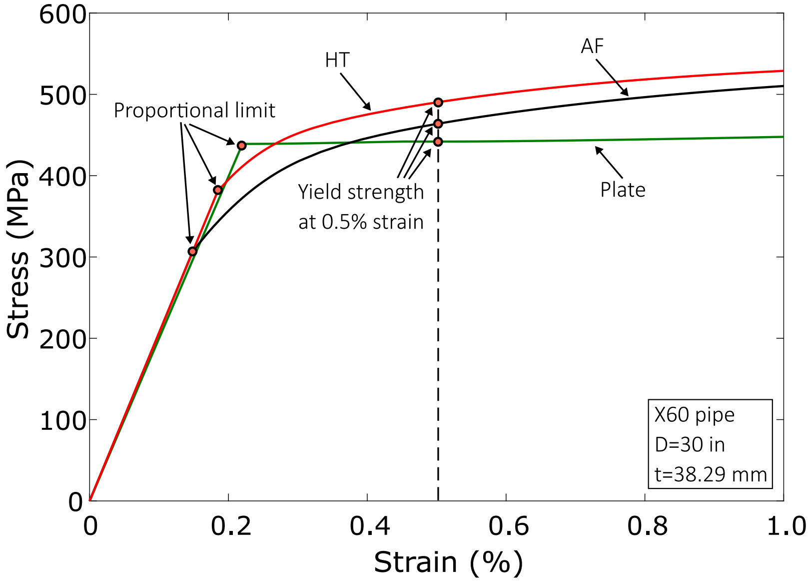

Fig. 20. Compressive stress–strain response in the circumferential direction (outer part), before (AF) and after heat treatment (HT), for the 30-inch-diameter X60 pipe; plate material response.

In Eq. (3), P_{el} is the critical elastic buckling pressure and P_p is the plastic pressure, expressed as follows:

$$P_{el} = \frac{2E}{\left(1-v^2\right)}\left(\frac{t}{D_o}\right)^3 \tag{4}$$

$$P_p = 2\sigma_{y,n}\alpha_{fab}\frac{t}{D_o} \tag{5}$$

where D_o and t are the outer diameter and wall thickness of the pipe, respectively, E, v and $\sigma_{y,n}$ are the Young's modulus, the Poisson's ratio and the specified minimum yield stress (SMYS) of the pipe material, O_o is the initial cross-sectional ovality of the pipe defined in Eq. (1) and α_{fab} is a fabrication factor, which accounts for the degradation of compression yield strength due to cold forming process. DNV-ST-F101 proposes a value of α_{fab} equal to 0.85 for expanded pipes (JCO-E or UOE). However, higher values of α_{fab} may be used with proper verification. The yield stress values (σ_y) of Table 1 are considered in DNV-ST-F101 formula for the "heat treated" (HT) and the "as fabricated" (AF) pipe. The average measured values of diameter and wall thickness, shown in Table 2, are used for each pipe. In this calculation, the value of initial ovality O_o is taken equal to 0.5%, which is the minimum value allowed by DNV-ST-F101.

The collapse pressure predictions for the two pipes under consideration are summarized in Table 3. The DNV-ST-F101 formula predictions are in fairly good agreement with the numerical and the experimental results, yet somewhat conservative. The collapse pressure from DNV-ST-F101 is also calculated with $\alpha_{fab} = 1$, to obtain a more realistic prediction of the collapse pressure for the heat treated pipes.

Finally, the numerical and experimental values of propagation pressure are compared with the corresponding prediction of DNV-ST-F101, denoted as P_{pr}, calculated from the following equation:

$$P_{pr} = 35\sigma_y\alpha_{fab}\left(\frac{t}{D_o}\right)^{2.5} \tag{6}$$

Table 4 summarizes the propagation pressure values from the full-scale experiment, the numerical analyses (capped end and fixed end conditions), and the DNV-ST-F101 formula predictions for the 30-inch pipe and the 24-inch pipe. Comparison of those values indicates that a value of α_{fab} equal to 0.85, in Eq. (6), results in conservative prediction of the propagation pressure compared to the experimental and numerical value. On the other hand, considering a fabrication factor (α_{fab}) equal to 1, a more realistic prediction of collapse pressure is obtained.

5. Parameter study

In the previous sections, experimental and numerical results indicated improvement of pipe collapse capacity under external pressure, because of partial compressive strength recovery of the pipe material due to mild heat treatment. In the present section, the three different compressive stress–strain curves considered in the previous sections, namely, the "plate material" curve, the "as fabricated" curve and the "heat treated" curve (Fig. 20), are employed to analyze the response of JCO-E pipes under uniform external pressure with different values of diameter-over-thickness ratio. The analyses assume fixed ends, which is a more realistic case for offshore pipelines.

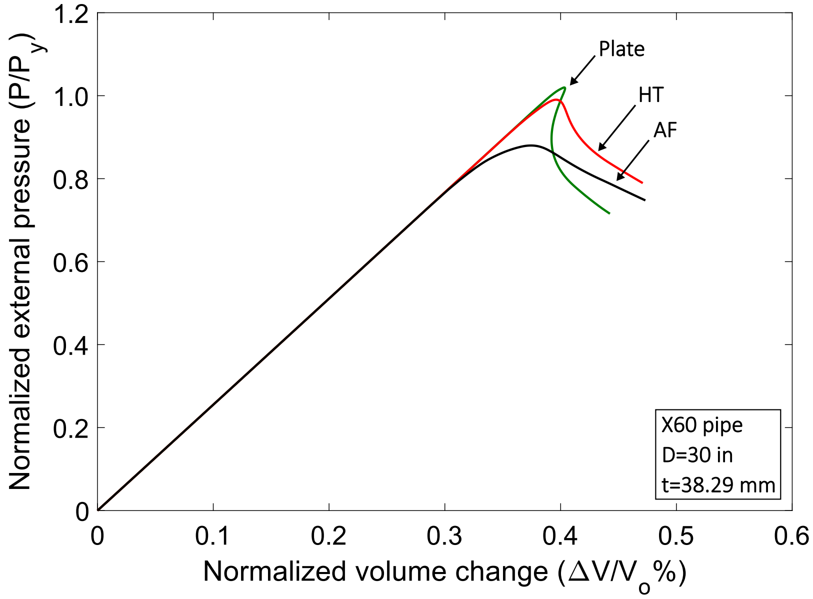

Fig. 21. External pressure versus volume change enclosed by the pipe, for the three different material curves of Fig. 20; 30-inch-diameter pipe.

5.1. *Effect of heat treatment parameters on material strength recovery*

Finite element analyses are performed with the stress–strain curves of Fig. 20, which are (a) the plate material behavior, fitted to the experimental stress–strain curve shown in Fig. 3 [9], (b) the "as fabricated" curve and (c) the "heat treated" stress–strain curve. The stress–strain curve of the plate may be assumed as the upper limit of material strength recovery, which theoretically corresponds to fully annealed material. The other two curves are described in Section 3.

The comparison between the stress–strain curves in Fig. 20 indicates a gradual increase of proportional limit and yield stress (σ_y) at 0.5% engineering strain. The proportional limit is 439 MPa for the plate, compared to 308 MPa and 381 MPa for the "as fabricated" and "heat treated" material, respectively, while the yield stress (σ_y) is 442 MPa for the plate, compared to 464 MPa and 490 MPa for the "as fabricated" and "heat treated" material, respectively. The yield stress of the plate is lower than the corresponding values of the other material curves, which is mainly attributed to material hardening after initial yielding.

The 14-diameter-long finite element model, presented in Section 4.2, is considered for simulating collapse and propagation, using the stress–strain curves of Fig. 20. Fig. 21 depicts the diagram of applied external pressure versus volume change for each material curve. The values of external pressure are normalized by the yield pressure of the pipe (Eq. (2)), where $\sigma_{y,n}$ is taken equal to the minimum specified yield stress of the X60 steel material (60 ksi or 414 MPa), D_o is the outer diameter of the 30-inch-diameter pipe and the volume change is normalized by the initial volume of the pipe segment V_o ($\Delta V/V_o$).

The numerical results verify that the collapse resistance of the pipes under consideration depends primarily on the compressive stress proportional limit in the circumferential direction. Using the "plate" stress–strain curve, the collapse pressure is equal to 44.6 MPa, significantly higher than the collapse pressure of the "as fabricated" pipe (38.5 MPa) and slightly higher than the collapse pressure of the "heat treated" pipe (43.4 MPa). Furthermore, the propagation pressure values corresponding to the three material curves are 8.4 MPa, 9.1 MPa and 9.3 MPa for the "plate", the "as fabricated" and the "heat treated" case, respectively. The lowest value of propagation pressure is obtained considering the "plate" material, and this is due to lack of hardening after initial yielding, while the "as fabricated" and the "heat treated" pipe materials result in similar predictions of propagation pressure. This is attributed to the approximately similar hardening of the two curves, as shown in Fig. 20.

5.2. *Influence of diameter-over-thickness ratio*

The effect of mild heat treatment and the associated aging process on collapse capacity and post-buckling performance is examined for pipes with different D/t values. A 30-inch-diameter pipe is considered with different wall thickness values, corresponding to D/t ratio values ranging from 15 to 25. The simulation follows the assumptions and steps presented in Section 3, in terms of material stress–strain curve, initial ovality, element type, mesh density. In this numerical study is assumed that the pipes despite their different D/t ratio have the same imperfections and material properties.

Fig. 22 summarizes the results of this parametric study and depicts the variation of collapse pressure with respect to the D/t value, ranging from 15 to 25, for "as fabricated" and "heat treated" pipes. The external pressure is normalized by the yield pressure in Eq. (2). Fig. 22 also presents the collapse pressure predictions from Eq. (3) proposed by DNV-ST-F101, assuming two values of

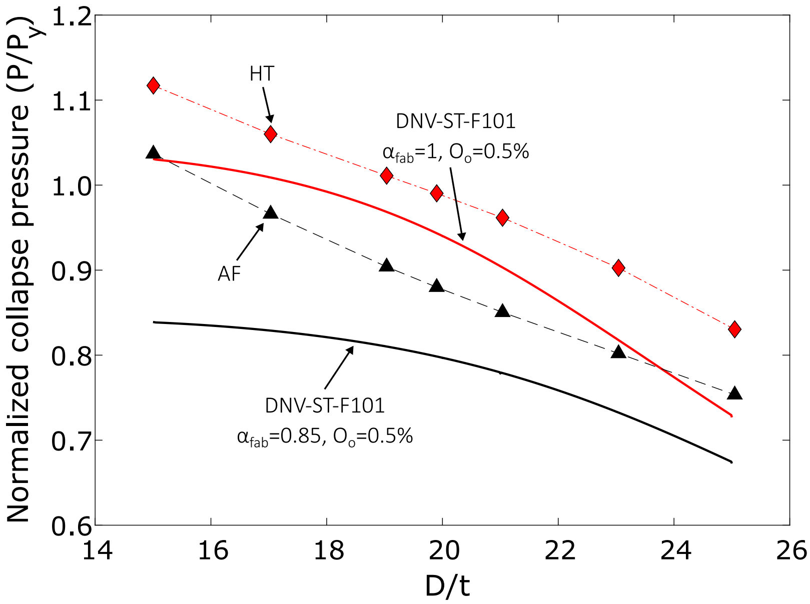

Fig. 22. External pressure variation with respect to D/t ratio, considering X60 material properties ("AF" and "HT").

Table 5
Numerical results of collapse and propagation pressure (in MPa) for different D/t values, using the experimental stress–strain curves before and after heat treatment.

D/t	Collapse pressure (MPa)		Propagation pressure (MPa)	
	AF	HT	AF	HT
15	61.2	66.0	17.7	18.2
17	49.9	54.7	13.0	13.3
19	41.5	46.4	9.8	10.1
20	38.5	43.4	9.1	9.3
21	35.1	39.7	7.7	7.8
23	30.1	33.9	6.1	6.3
25	25.9	28.6	5.1	5.1

the fabrication factor (α_{fab}), namely 0.85 and 1. The latter value accounts for material strength recovery after heat treatment, as discussed in more detail in Section 4.3. The comparison between numerical results and DNV-ST-F101 predictions indicates a slight underprediction of collapse pressure obtained by the DNV-ST-F101 formula (Eq. (3)), for both values of α_{fab} (0.85 and 1). This is mainly attributed to the value of initial cross-sectional ovality ($O_o = 0.5\%$) considered by the standard, which is significantly higher than the ovality value measured in the JCO-E pipe under consideration.

The collapse pressure P_c and propagation pressure P_{pr} are summarized in Table 5 for the D/t range of interest. The values of P_c and P_{pr} decrease with increasing D/t ratio. Furthermore, the collapse pressure after heat treatment is consistently higher by an average of 11% for the D/t range of interest. On the other hand, the value of propagation pressure is almost unaffected by heat treatment for the entire range of D/t values, and this is attributed to the similar slope of material hardening in the "as fabricated" and the "heat treated" stress–strain curves, also noticed in Section 5.1

Finally, numerical analyses are performed for the highest and the lowest D/t values (15 and 25), using the compressive material curves of Fig. 20, and the pressure–volume diagrams are shown in Fig. 23. For $D/t = 25$, the collapse pressure for the "plate" material is equal to 29.3 MPa, compared to 25.9 MPa and 28.6 MPa for the "as fabricated" and the "heat treated" cases, respectively. The numerical results indicate that the proportional limit of the material curve is the main parameter affecting the collapse pressure of this pipe. On the contrary, for the thick-walled pipe ($D/t = 15$), the "heat treated" pipe exhibits the maximum collapse pressure. In this case, the collapse capacity appears to be influenced both by the value of proportional limit and by material hardening. The "as fabricated" pipe exhibits the lowest collapse pressure in both D/t cases (15 and 25). The values of collapse and propagation pressure are summarized in Table 6.

6. Conclusions

The application of mild heat treatment, corresponding to a typical coating process, increases the compressive circumferential strength of the line pipe material, and reduces the effect of cold bending and expansion on the compressive yield strength of the

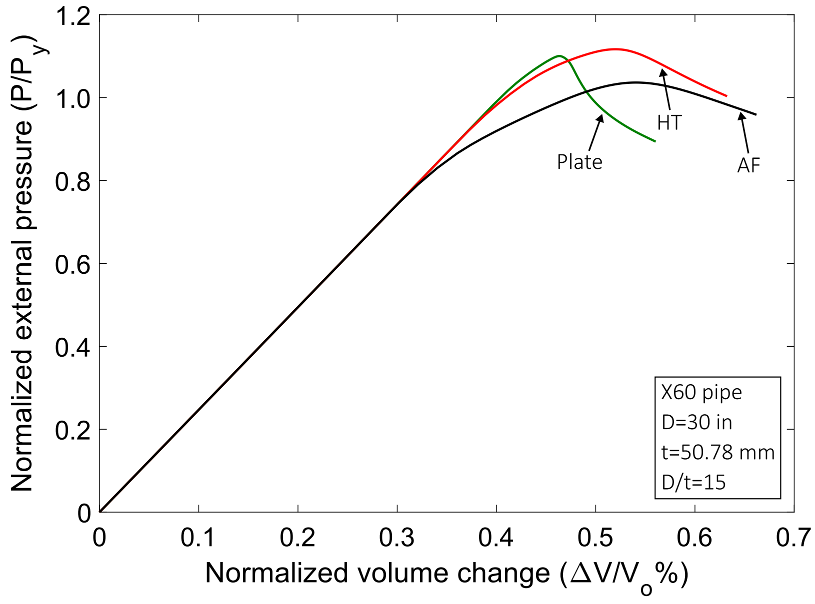

(a)

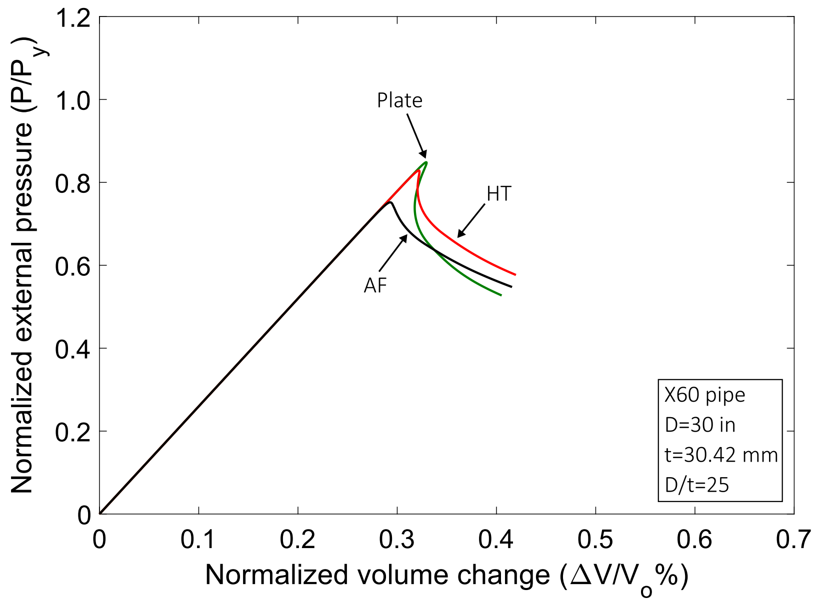

(b)

Fig. 23. External pressure vs. volume change diagram; (a) $D/t = 15$ and (b) $D/t = 25$, considering the three different material curves of Fig. 20.

pipe material. Results from uniaxial compression tests in the hoop direction of the pipe show an increase of about 5% in the yield stress and 24% in the proportional limit for the X60 and X65 pipe materials under consideration.

The use of circumferential stress–strain compression curves measured at the outer pipe part, provides very good predictions of collapse pressure compared to full-scale experiments. Direct comparison between the numerical results of the collapse pressure before and after heat treatment shows that the value of collapse pressure increases by approximately 13%-15% for the pipes under consideration, verifying the beneficial effect of heat treatment (similar to the typical heating conditions for the application of a 3-layer coating system) on their collapse resistance. The numerical and experimental results of the collapse pressure are also compared with the corresponding predictions of DNV-ST-F101. The so-called fabrication factor (α_{fab}), introduced by DNV-ST-F101 to account for the effects of pipe fabrication, has an important influence on the predicted value of collapse pressure. The standard

Table 6
Collapse and propagation pressure (in MPa) of 30-inch X60 pipes with two D/t values, using different material stress–strain curves.

Level	Collapse pressure (MPa)		Propagation pressure (MPa)	
	$D/t = 15$	$D/t = 25$	$D/t = 15$	$D/t = 25$
Plate	65.0	29.3	16.5	4.7
Before HT	61.2	25.9	17.7	5.1
After HT	66.0	28.6	18.2	5.1

provides reliable yet conservative predictions of collapse pressure before and after heat treatment, when an appropriate value of fabrication factor is considered. In particular, to obtain reliable estimate of collapse pressure for the heat treated JCO-E pipes under consideration, the fabrication factor should be equal to 1.

The influence of partial material strength recovery on the collapse strength of a 30-inch-diameter pipe with D/t approximately equal to 20 is examined. The results highlight the strong dependence of pipe collapse pressure on the value of proportional stress limit of the stress–strain curve. Heat treatment increases the proportional limit of the material curve and results in higher collapse pressure than the “as fabricated” pipe. The highest collapse pressure is obtained considering the stress–strain curve of the plate material, which has the highest proportional limit. On the other hand, the values of propagation pressure are only slightly affected by this mild heat treatment due to similar hardening of the “as fabricated” and “heat treated” material curves.

The collapse performance of pipes with D/t values ranging from 15 to 25 has also been examined. The collapse pressure increases with decreasing D/t ratio, while the collapse pressure of “heat treated” pipes is consistently higher than the collapse pressure of “as fabricated” pipes for the entire range of D/t ratios considered. The results also indicate that for thinner pipes (e.g. $D/t = 25$) the proportional limit is the main contributing factor for the collapse pressure. For thicker pipes ($D/t = 15$), the collapse pressure also depends on material hardening.

The results of the present paper are based on testing and analysis of JCO-E pipes. Nevertheless, the main conclusions in terms of compressive strength degradation due to cold bending and expansion, and the beneficial effect of mild heat treatment on collapse pressure are also applicable to other types of welded/expanded pipe (e.g., UOE).

Declaration of competing interest

The authors declare that they have no known competing financial interests or personal relationships that could have appeared to influence the work reported in this paper.

Data availability

Data will be made available on request.

Acknowledgments

The authors would like to thank Corinth Pipeworks S.A., Greece for their financial support, and their permission for publishing this paper. Many thanks also go to C-FER Technologies, and in particular to Doug Swanek and Chris Timms for performing the full-scale collapse tests.

References

[1] Kyriakides S, Corona E. Mechanics of Offshore Pipelines: Volume 1 Buckling and Collapse, Vol. 1. Elsevier; 2007.
[2] Kyriakides S, Lee LH. Mechanics of Offshore Pipelines, Volume 2: Buckle Propagation and Arrest. Gulf Professional Publishing; 2020.
[3] Karamanos SA. Structural Mechanics and Design of Metal Pipes, a Systematic Approach for Onshore and Offshore Pipelines. first ed.. Elsevier; 2022.
[4] Palmer AC, Martin JH. Buckle propagation in submarine pipelines. Nature 1975;254(5495):46–8.
[5] Antoniou K, Chatzopoulou G, Karamanos SA, Tazedakis A, Palagas C, Dourdounis E. Numerical simulation of JCO-E pipe manufacturing process and its effect on the external pressure capacity of the pipe. J Offshore Mech Arct Eng 2019;141(1):011704.
[6] Kyriakides S, Corona E, Fischer F. On the effect of the UOE manufacturing process on the collapse pressure of long tubes. In: Offshore Technology Conference. OTC-6758-MS; 1991.
[7] Stark PR, McKeehan DS. Hydrostatic collapse research in support of the oman India gas pipeline. In: Offshore Technology Conference. Houston, Texas, USA: OTC-7705-MS; 1995.
[8] Herynk MD, Kyriakides S, Onoufriou A, Yun HD. Effects of the UOE/UOC pipe manufacturing processes on pipe collapse pressure. Int J Mech Sci 2007;49(5):533–53.
[9] Antoniou K. Numerical Simulation of JCO-E Line Pipe Manufacturing and Its Influence on the Mechanical Behavior and Strength of Offsore Pipelines [Ph.D. thesis], Department of Mechanical Engineering, University of Thessaly; 2021.
[10] Reichel T, Pavlyk V, Beissel J, Kyriakides S, Jang W-Y. New Impander technology for improved collapse resistance of large diameter pipe for deepwater applications. In: Offshore Technology Conference. Houston, Texas, USA: OTC-21503-MS; 2011.
[11] Al-Sharif AM, Preston R. Improvement in UOE Pipe Collapse Resistance by Thermal Aging. In: Offshore Technology Conference, Houston, Texas, USA. OTC-8211-MS; 1996.

[12] DeGeer D, Marewski U, Hillenbrand HG, Weber B, Crawford M. Collapse testing of thermally treated line pipe for ultra-deepwater applications. In: Proceedings of the ASME 2004 23rd International Conference on Offshore Mechanics and Arctic Engineering. Vancouver, British Columbia, Canada: OMAE2004-51569; 2004.
[13] Shinohara Y, Hara T, Tsuru E, Asahi H, Terada Y, Doi N. Change of mechanical properties of high strength line pipe by thermal coating treatment. In: Proceedings of the ASME 2005 24th International Conference on Offshore Mechanics and Arctic Engineering. Halkidiki, Greece: OMAE2005-67055; 2005.
[14] DeGeer D, Timms C, Lobanov V. Blue Stream Collapse Test Program. In: Proceedings of the ASME 2005 24th International Conference on Offshore Mechanics and Arctic Engineering. Halkidiki, Greece: OMAE2005-67260; 2005.
[15] Arroyo F, Solano RF, Mantovano L, de Azevedo FB, Alves H, Swanek D, et al. Qualification of UOE SAWL linepipes with enhanced collapse resistance for ultra deepwater applications. In: Proceedings of the ASME 2013 32nd International Conference on Ocean, Offshore and Arctic Engineering, Nantes, France. OMAE2013-10957; 2013.
[16] Serebrinsky S, Mantovano L, Arroyo F, Valdez M, Ernst H, Silva R. Material Testing for the Prediction of the Effect of Deformation and Aging Thermal Treatments on Collapse Resistance of UOE Pipes. In: Proceedings of the ASME 2013 32nd International Conference on Ocean, Offshore and Arctic Engineering, Nantes, France. OMAE2013-11394; 2013.
[17] De Lucca R, Solano RF, Swanek D, de Azevedo FB, Arroyo F, Alves H, et al. Enhanced collapse resistance for different D/t ratios of UOE pipes for ultra deepwater application. In: International Conference on Offshore Mechanics and Arctic Engineering, Volume 5B: Pipeline and Riser Technology, 2015.
[18] Gavriilidis I, Stamou AG, Tazedakis A, Voudouris N, Palagas C, Dourdounis E, et al. Collapse testing and analysis of JCO-E steel pipes. In: Proceedings of the 17th Pipeline Technology Conference. Berlin, Germany; 2022.
[19] Det Norske Veritas. Submarine pipeline systems. 2021, standard DNV-ST-F101, H≇vik, Norway.
[20] Hibbitt H, Karlsson B, Sorensen P. ABAQUS: Theory manual, version 2016. 1992, Dassault Systèmes Simulia Corp, Providence, RI.
[21] Toscano RG, Timms CM, Dvorkin EN, DeGeer DD. Determination of the collapse and propagation pressure of ultra-deepwater pipelines. In: Proceedings of the ASME 2003 22nd International Conference on Offshore Mechanics and Arctic Engineering. Cancun, Mexico: OMAE2003-37339; 2003.